Chapter 6 In situ growth of Cu_2S/TiO_2 heterojunction for visible-NIR photodetector

6.1 Introduction

In the last two decades, a large number of works have been reported on nanocrystal based UV-visible-NIR photodetectors [153, 154]. A variety of different nanocrystals including colloidal quantum dot, [155] 2D semiconductors, [156] metal oxide semiconductor nanocrystal [157, 158] have been used as photoactive material of those devices. Among them, lower bandgap colloidal quantum dot has been used particularly for developing NIR photodetectors [159, 160]. On the other hand, 2D semiconductors and wide band-gap metal-oxide nanocrystal are used for broadband photodetectors[161, 162] and UV detector respectively [163]. All of these different photodetectors have different applications including communication, [164] imaging, [165] biological sensor, [166] water purification system, etc. These nanocrystals based photodetectors have advantages like particle size-dependent bandgap tunability, solution processability, low cost etc. [167]. However, for practical applications, photodetectors should have high detectivity with good response speed and high stability.

Cuprous sulfide (Cu_2S) is a well-known p-type semiconductor with a bandgap of 1.6 eV which can be a suitable choice for visible light-sensitive photodetector fabrication. Earlier, several efforts have been given to fabricate Cu_2S based heterojunction photodetector. However, the responsivity and detectivity of these Cu_2S based photodetectors are still quite poor [168-171]. In our present work, a unique approach has been taken to develop Cu_2S NPs within titanium oxide (TiO_2) thin film and has been utilized for efficient visible light photodetector application. This thin film growth consists

of two successive steps including sol-gel derived ion-conducting $Li_4Ti_5O_{12}$ (LTO) thin-film fabrication containing loosely bound light ion (Li^+) followed by ion-exchanged (with Cu^+) and subsequent sulfurization process. In this process, large area Cu_2S-TiO_2 thin film containing Cu_2S NPs with a particle size ranging from 10 to 60 nm were readily obtained. The electrical conductivity of this Cu_2S-TiO_2 thin film was highly enhanced under the illumination of white light, indicates its high photosensitivity to the visible-NIR region. This photosensitivity can be enhanced further with an additional ZnO layer that encourages us to fabricate Cu_2S-TiO_2/ZnO lateral heterojunction photodetector. This heterojunction photodetector shows significantly higher photo-detectivity with respect to the individual Cu_2S-TiO_2 and ZnO photodetectors.

6.2 Results and Discussions

6.2.1 Structural and Surface morphology characterization

Crystal phases of $Li_4Ti_5O_{12}$, Cu_2S, and TiO_2, have been identified through X-ray diffraction (XRD) study. Initially, a drop cast sample of $Li_4Ti_5O_{12}$has been prepared on a glass substrate followed by ion-exchange and sulfurization processes that have been followed for Cu_2S-TiO_2 thin film sample preparation. **Figure 6.1(a)** shows the XRD pattern of the $Li_4Ti_5O_{12}$ and Cu_2S-TiO_2 samples. The diffraction peaks of $Li_4Ti_5O_{12}$ are located at $2\theta \sim 18.5, 35.6, 43.7$ that are associated with reflection planes of (111), (311) and (331) respectively, indicates its cubic spinel structure with the space group of ($F\bar{3}dm$) (JCPDS file no. 490207). After complete reaction, $Li_4Ti_5O_{12}$ structure is changed into Cu_2S-TiO_2 nanocomposite that has been identified with XRD data with a diffraction peak that appeared at $2\theta \sim 25.35$ for anatase phase of this TiO_2. This TiO_2 phase shows the tetragonal structure with space group $I4_{1/amd}$ (JCPDS no. 894921). In addition, the diffraction peaks of

Cu_2S have appeared at 2θ ~37.66 and 45.70 due to the reflection planes of (102) and (110) respectively which ensure the hexagonal structure of Cu_2S with $P6_3/mmc$ space group (JCPDS no. 261116).

Figure 6.1(b) shows the normalized UV-VIS absorption spectra of pure $Li_4Ti_5O_{12}$, TiO_2, and Cu_2S-TiO_2 thin film covering the optical range of 350-900 nm. Absorption spectra of Cu_2S-TiO_2 thin film show broadening of original $Li_4Ti_5O_{12}$ absorption, which is due to the low bandgap Cu_2S NPs formation inside the TiO_2 film. This extended absorption is useful for visible light photodetector applications.

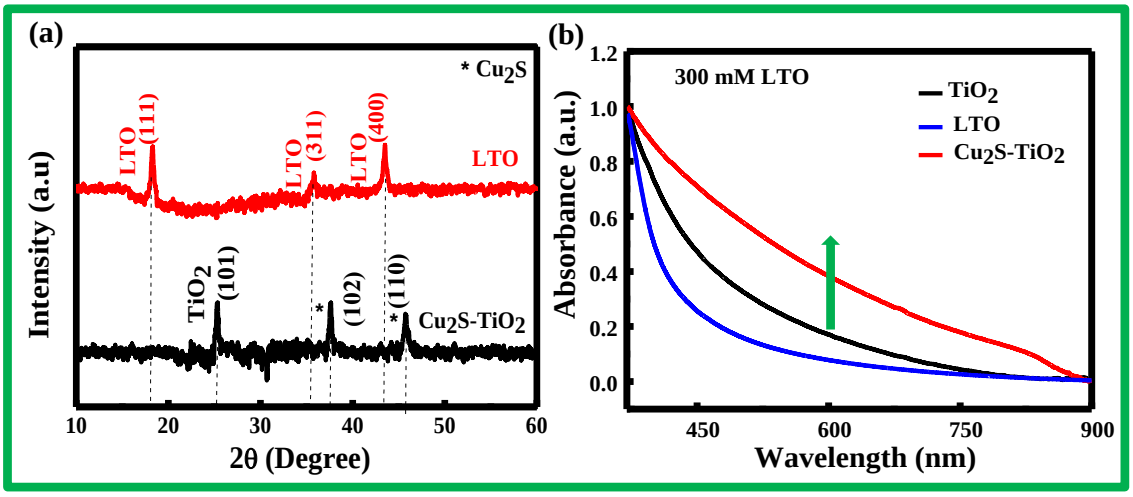

Figure 6.1: The XRD pattern of (a) Cu_2S- TiO_2 and pure LTO (b) UV-Vis spectra of LTO, TiO_2, and Cu_2S- TiO_2 thin films.

6.2.2 The Surface morphology characterization

The detail of the surface morphology of Cu_2S (NPs)-TiO_2 was investigated by high resolution-scanning electron microscopy (HR-SEM), which has been shown in **figure 6.2(a)**. The sample was prepared on a glass substrate by spin coating with a speed of 4500 rpm, followed by the same ion-exchange and sulfurization process.

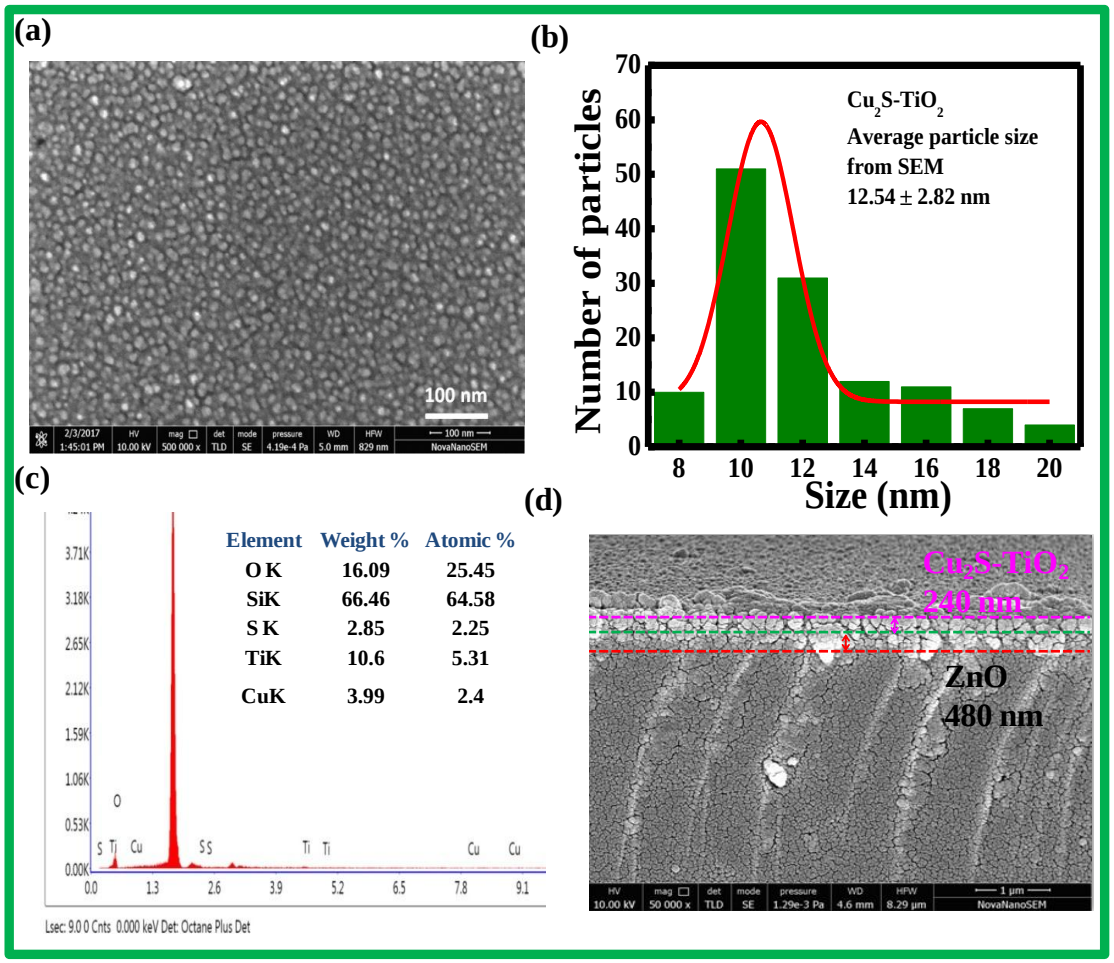

Figure 6.2 *(a) SEM image of Cu_2S-TiO_2 thin film (b) Size distribution of Cu_2S NPs inside TiO_2 thin film fromscanning electron microscope (c) The elemental and composition analysis show the spectrum and inset show the table of Cu_2S-TiO_2,(d) The cross section image of the deviceCu_2S-TiO_2/ZnO/Glass.*

The SEM image of the Cu_2S (NPs)-TiO_2 thin film indicates the different contrast of Cu_2S nanocrystal formation inside the TiO_2 matrix. Additionally, it gave the information about the size of Cu_2S NPs, which is within the range from 8 to 20 nm with an average particle size of 12.5 nm. The distribution of particle size has been given in **figure 6.2(b)**. The composition and content of the metallic element were determined by an energy- dispersive X-ray spectrometer (EDX) attached to the HR-SEM. This picture clearly shows the existence of Cu and Ti elements inside the thin film **(figure 6.2(c)**.

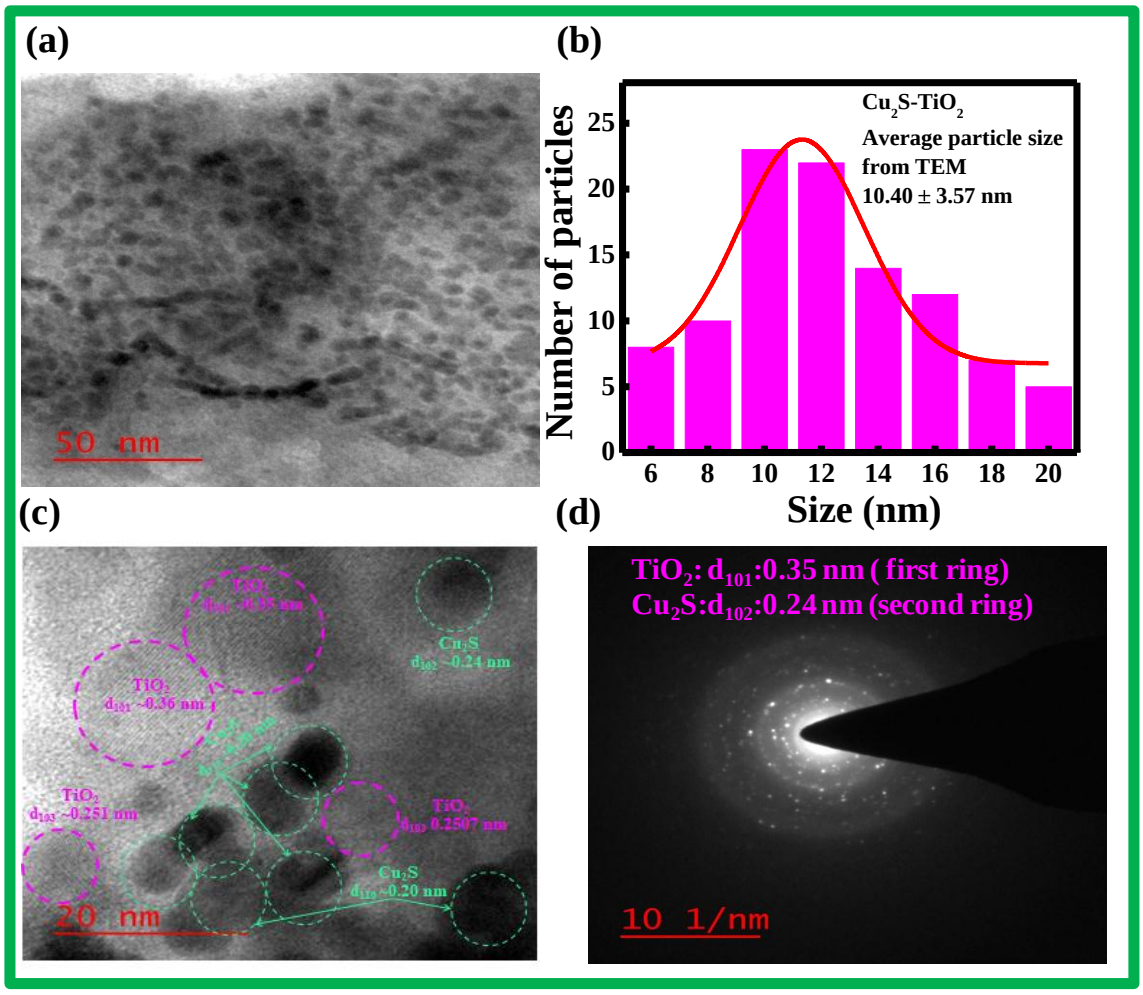

Figure 6.3: *(a) The TEM image of Cu_2S-TiO_2,(b) Size distribution of Cu_2S NPs inside TiO_2 thin film from TEM image (c) High resolution TEM image of Cu_2S (NPs)-TiO_2, the greenish circle indicates the lattice d-fringe of Cu_2S and pink circle for TiO_2 (d)Selected area diffraction pattern of Cu_2S (NP)-TiO_2.*

Cross-sectional SEM study of Cu_2S (NPs)-TiO_2/ZnO photodetector indicates that the thickness of ZnO is ~480 nm and Cu_2S (NPs)-TiO_2 ~240 nm **(figure 6.2(d).**

The more detail of structural analysis Cu_2S (NPs)-TiO_2 heterostructure has been studied by transmission electron microscopy (TEM), which is shown in **figure 6.3(a)**. For the sample preparation of this experiment, Cu_2S-TiO_2 thin film was separated from the substrate and made a fine powder by using a grinding mortar that was dispersed in chloroform by keeping the solution under ultrasonic bath for 1 hour. As shown in **figure**

6.3(a), Cu_2S-NPs are grown inside the TiO_2 matrix quite uniformly. This picture also shows that the particle size is distributed mostly within the range 6-20 nm with an average particle size of 10.4 nm which is very similar to SEM study. The particle size distribution of Cu_2S NPs has been shown in **figure 6.3(b)**, which is also very much similar to SEM analysis. Higher magnification image (**Figure 6.3(c)** of Cu_2S NPs-TiO_2 shows the lattice fringe formation of Cu_2S-NPs and TiO_2 individually indicates their co-existence. The measured averaged d-spacing of Cu_2S-NPs and TiO_2 are 0.24 and 0.35 nm respectively that are corresponding to Cu_2S (102) and anatase TiO_2 (101) plans and these d spacing are also identified with selected area electron diffraction pattern (SAED) which is shown in **figure 6.3(d).** The XRD analysis of Cu_2S-TiO_2 sample **(Figure-6.1(a))** has also recognized these two planes of Cu_2S and TiO_2 that have been discussed earlier.

6.2.3 Electrical properties

The electrical current-voltage (I-V) characteristics of single-layer and bilayer heterojunction photoconductors have been performed under dark and white light illumination as shown in figure 6.4. High power Xenon light has been used as a white light source and the device was illuminated from the top side of the device as shown inset of figure 6.4 (a & b). The comparative I-V characterization ZnOonly device, and Cu_2S-TiO_2/ZnO heterojunction device shown in figure 6.4 (a & b). This study shows that bilayer Cu_2S-TiO_2/ZnOheterojunction generates the highest photocurrent with the largest difference between photo-to-dark current with a value of 1.1 mA/cm^2 as shown in figure 6.4(a). The schematic presentation of relative band alignment, band bending and charge separation of ZnO only and Cu_2S-TiO_2/ZnOheterostructure photodetector devices are shown in figure 6.4(c & d). In the heterojunction devices, wide band gap ZnO (3.4 eV)

works as lateral charge transport layer whereas comparatively narrower band gap Cu_2S NPs (~1.5 eV) performs as active light absorbing layer. Therefore, photo-generated excitons are formed within the Cu_2S NPs as shown in figure 6.4(c). Subsequently, photo-generated excitons are separated into electrons and holes by the electric field formed due to the junction potential of Cu_2S-TiO_2/ZnO interface. The electrons are transferred to ZnO layer by increasing the conductivity of ZnO layer as shown in figure 6.4(c). On the other hand, while holes remain in the Cu_2S-TiO_2 film, thus resulting in an increase in the total conductivity of the devices [172]. Such kind of lateral heterojunction device offers higher photocurrent over single-layer device predominantly due to (i) the physical separation of photogenerated electron and hole in two different semiconducting layers, (ii) lesser trap assisted recombination at the substrate/semiconductor interface owing to physical separation of carriers from substrate by the intermediate charge transport layer, and (iii) higher electron mobility in ZnO layer.

The responsivity R_λ and detectivity (D*) are the key figure of the merits of a photodetector that can be determined by measuring from External Quantum Efficiency (EQE) and dark current. The values of R_λ and EQE are related by following equations,

$$R_\lambda = \frac{\Delta I_\lambda}{P_\lambda S} \tag{6.1}$$

$$EQE = \frac{hcR_\lambda}{e\lambda} \tag{6.2}$$

where, ΔI_λ is the difference between photocurrent and dark current, P_λ is the incident light intensity, S is the effective illuminated area, h is Planck's constant, c is the velocity of light, e is the electronic charge and λ is the excitation wavelength. Figure 6.5(a) shows the measured EQE of the photoconductor for different external biases. This data indicates

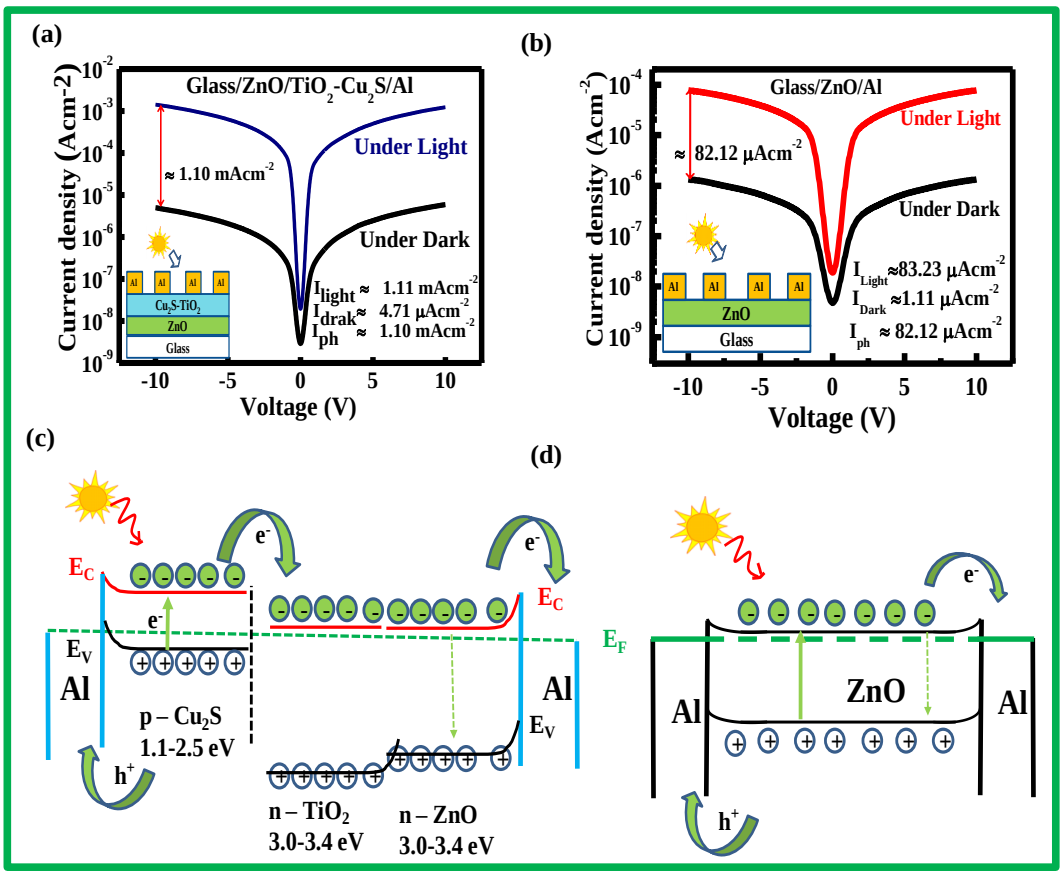

Figure 6.3(a-b) Semi log plot shows the photoconductivity of a)Glass/ZnO/TiO_2-Cu_2S/Al, b) Glass/ZnO/Al under dark and light conditions. Band alignment, band bending, and charge separation of (c) Al/Cu_2S-TiO_2/ZnO (d) Al/ZnOheterostructure photodetector devices.

broadband photosensitivity over a range of 350-900 nm as well as gradual enhancement of EQE with external bias. As shown in figure 6.5(a), EQE increases up to 33% at 830 nm under 10V external bias due to increasing gain in the photoconductor. Similarly, responsivity of the device increases under external bias with a value of 0.22 (A/W) at 830 nm under 10 V bias which is shown in figure 6.5(b). The detective (D*) of the device has been measured by the signal-to-noise ratio of photodetector over a 1 Hz bandwidth normalized to the detector area. It is the most important figure of merit of photodetector

that allows for sensitivity comparison among detectors of different geometries [24,172, 173].

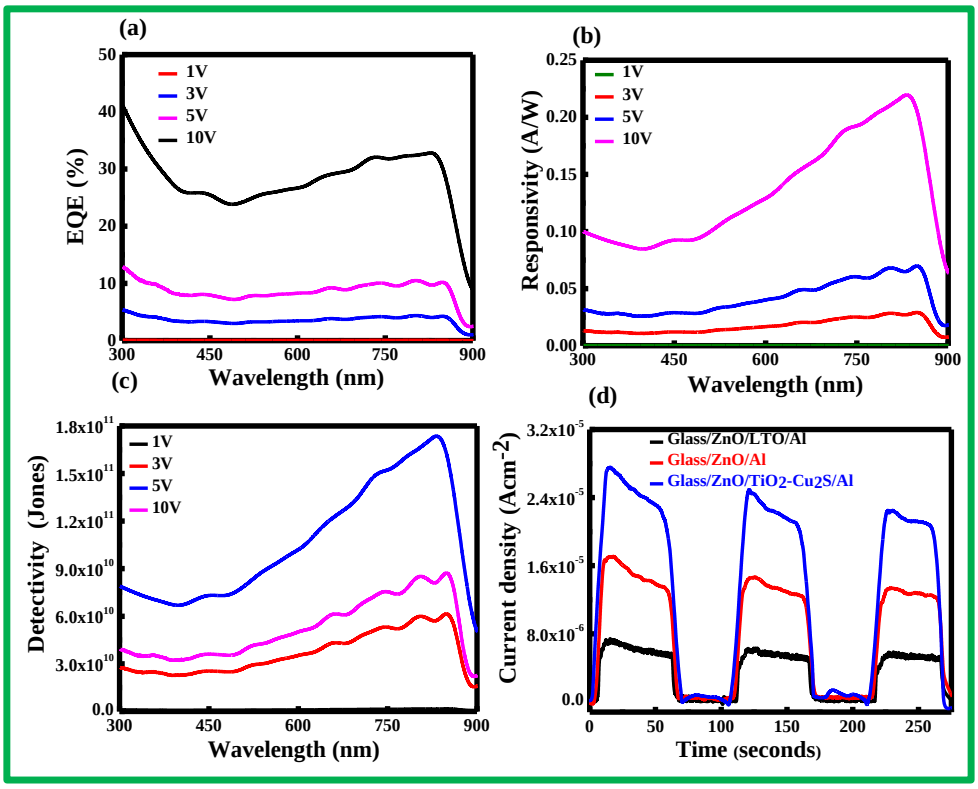

Figure 6.4: *Cu_2S-TiO_2/ZnO lateral heterojunction photoconductor device performance (a) External quantum efficiency (EQE) vs. Wavelength, (b) Extracted responsivity vs wavelength (c) Extracted detectivity vs wavelength and (d) Transient time response of these same set of devices structures Glass/ZnO/TiO_2-Cu_2S/Al, Glass/ZnO/LTO/Al, and Glass/ZnO/Al.*

In our calculation, we are assuming the shot noise, which originated from the dark current, has a major contribution to the total noise current of the photodetector. Therefore, the detectivity of the device is then given by equation.

$$D^* = R_\lambda/(2eJ_d)^{1/2} \qquad (6.3)$$

Where, J_d is the dark current density. Figure 6.5(c) shows the detectivity (D*) data at a different frequency range that exhibits the highest detectivity of 1.7×11^{11} jones upon illumination of 830 nm light.

Table 1: The rising and falling time of the three different device structures shown in the table.

Device	Raising time (Seconds)	Decay time (Seconds)
Glass/ZnO/LTO/Al	10.12	12.01
Glass/ZnO/Al	10.24	32.14
Glass/ZnO/ TiO_2-Cu_2S/Al	7.11	8.21

Table 2: A table has been provided for comparison with other chalcogenide nanoparticle based photodetector.

Device	Responsivity [A W^{-1}]	EQE [%]	Detectivity [cm $Hz^{1/2}W^{-1}$]	Wavelength[nm]	Ref.
Cu_2S-TiO_2	**0.22 A/W**	**33**	1.7×11^{11}	**830**	**This work**
ZnO/PbS	4.19	742	1.07×10^{11}	350-900	*ACS Appl. Nano Mater***1**, 6063–6072 (2018)
Bi_2Te_3-SnSe-Bi_2Te_3	5.5	1833	6×10^{10}	370–808	*Adv. Funct. Mater.***27**, 1701823 (2017)
Gr-WS_2-Gr	3.5	933	1.6×10^{10}	532	*ACS Appl. Mater. Interfaces* **9**, 5392–5398 (2017)
Gr-WS_2-Gr	0.1	30	NA	488–633	*Science (80).***275**, 1102–1106 (1997)
Gr-$MoTe_2$-Gr	0.205	53.8	NA	473–1064	*Nat. Nanotechnol.***6**, 45–50 (2011)
Ag-SnSe-Ag	8.8×10^{-8}	2.3×10^{-7}	8.7×10^{5}	473	Nanotechnology 25, 105705 (2014)
ITO-SnSe-ITO	6×10^{-6}	NA	1.8×10^{7}	White light	*Mater. Res. Express* **3**, 105038 (2016)
Ti-SnSe/WS_2-Ti	0.099	26	1.2×10^{8}	473–1064	*ACS Appl. Mater. Interfaces* **8**, 4781–4788 (2016)

The transient time response is another important parameter of the photoconductors and this transient response of these devices is shown in figure 6.5(d). This measurement was performed at the 5 volts external biasing with one sun white light illumination. This data shows quite a fast rise and fall time response of all devices. However, a device with device structure glass/ZnO/Cu_2S-TiO_2 shows a slightly faster response due to the batter interface formation of ZnO with Cu_2S-TiO_2 thin film that creates less number of carrier trap state at the interface. The values of rising and fall time of the devices are summarized in table 6.1.

6.3 Conclusions

Heavy metal-free, narrow bandgap nanoparticle of Cu_2S has been grown inside TiO_2 thin films by a solution-processed technique that allows us to deposit large area uniform Cu_2S- TiO_2 heterojunction thin film. The particle size of Cu_2S was estimated from the HR-SEM image which is in the range of 8-20 nm. This electronically coupled Cu_2S-TiO_2 heterojunction thin film shows very high photosensitivity in visible light. A photodetector of Cu_2S- TiO_2 thin film with an underlying ZnO layer has been fabricated with a device architecture of glass/ZnO/TiO_2-Cu_2S/Al that shows the responsivity and detectivity of 0.22 A/W and 1.7×10^{11} jones respectively at 830 nm. The transient time response study of this device shows that the rising and falling time of these devices is 7.1 and 8.2 seconds respectively, which is reasonable good for photoconductor devices.